

THE 5.25 AND 5.7 μm ASTRONOMICAL POLYCYCLIC AROMATIC HYDROCARBON EMISSION FEATURES*

C. BOERSMA¹, A. L. MATTIODA^{2,3}, C. W. BAUSCHLICHER JR.⁴, E. PEETERS^{3,5}, A. G. G. M. TIELENS^{1,2}, AND L. J. ALLAMANDOLA²

¹ Kapteyn Astronomical Institute, University of Groningen, P.O. Box 800, 9700 AV, Groningen, The Netherlands; C.Boersma@astro.rug.nl

² NASA Ames Research Center, MS 245-3, Moffett Field, CA 94035, USA

³ SETI Institute, 515 N. Whisman Road, Mountain View, CA 94043, USA

⁴ NASA Ames Research Center, MS 230-3, Moffett Field, CA 94035, USA

⁵ Department of Physics and Astronomy, PAB 213, The University of Western Ontario, London, ON N6A 3K7, Canada

Received 2008 June 28; accepted 2008 September 1; published 2008 December 8

ABSTRACT

Astronomical mid-IR spectra show two minor polycyclic aromatic hydrocarbon (PAH) features at 5.25 and 5.7 μm (1905 and 1754 cm^{-1}) that hitherto have been little studied, but contain information about the astronomical PAH population that complements that of the major emission bands. Here, we report a study involving both laboratory and theoretical analysis of the fundamentals of PAH spectroscopy that produce features in this region and use these to analyze the astronomical spectra. The *Infrared Space Observatory* Short Wavelength Spectrograph spectra of 15 objects showing these PAH features were considered for this study, however only four (HD 44179; NGC 7027; Orion Bar, two positions) have sufficient signal-to-noise between 5 and 6 μm to allow for an in-depth analysis. All four astronomical spectra show similar peak positions and profiles. The 5.25 μm feature is peaked and asymmetric, with an FWHM of about $0.12 \pm 0.01 \mu\text{m}$ ($\sim 40 \pm 6.5 \text{ cm}^{-1}$), while the 5.7 μm feature is broader and flatter, with an FWHM of about $0.17 \pm 0.02 \mu\text{m}$ ($50 \pm 5.6 \text{ cm}^{-1}$). Detailed analysis of the laboratory spectra and quantum-chemical calculations show that the astronomical 5.25 and 5.7 μm bands are a blend of combination, difference and overtone bands primarily involving CH stretching and CH in-plane and CH out-of-plane bending fundamental vibrations. The experimental and computational spectra show that, of all the hydrogen adjacency classes that are possible on PAHs, solo and duo hydrogens consistently produce prominent bands at the observed positions, whereas quartet hydrogens do not. In all, this study supports the picture that astronomical PAHs are large with compact, regular structures. From the coupling with primarily strong CH out-of-plane bending modes, one might surmise that the 5.25 and 5.7 μm bands track the neutral PAH population. However, theory suggests that the role of charge in these astronomical bands might also be important.

Key words: astrochemistry – ISM: lines and bands – methods: laboratory – methods: numerical – molecular data – techniques: spectroscopic

Online-only material: extended figures

1. INTRODUCTION

Some 30 years of observations, combined with computational and laboratory studies, have shown that the mid-IR astronomical emission features, formerly referred to as the unidentified IR (UIR) bands, are produced by mixtures of highly vibrationally excited polycyclic aromatic hydrocarbons (PAHs) and closely related species. Detected in many Galactic and extragalactic objects, including several with significant redshift (e.g., Yan et al. 2005), the astronomical IR emission features present an important and unique probe of astrochemical and astrophysical conditions across the universe. Recent reviews and papers of the observational and laboratory work (e.g., Peeters et al. 2004; Hudgins & Allamandola 2004; van Dishoeck 2004; Sellgren et al. 2007; Smith et al. 2007; Tielens 2008) and work on theoretical models (e.g., Verstraete et al. 2001; Bakes et al. 2001; Li & Draine 2001; Pech et al. 2002; Rapacioli et al. 2006; Draine & Li 2007) can be found elsewhere.

The major features at 3.3, 6.2, “7.7,” 8.6, and the complex of bands between 11 and 20 μm have been studied in great detail (e.g., Van Kerckhoven et al. 2000; Hony et al. 2001; Peeters et al. 2002; van Diedenhoven et al. 2004, and references

therein), and the fundamental spectroscopic information with which one can analyze the strongest astronomical features is now available. However, there are several components of the astronomical PAH emission spectra that have been widely overlooked. Many of these contain valuable, sometimes subtle, information which is equally important to that revealed by the more well-known features. This study focuses on such features, namely the weak bands that fall between 5 and 6 μm (2000 and 1667 cm^{-1}).

One of the early predictions of the PAH hypothesis was the expectation of a weak emission feature near 5.25 μm in all objects showing the major PAH bands. Its detection in 1989 (Allamandola et al. 1989a) was an early confirmation of the PAH hypothesis. Since that time, although evident in many spectra showing the major PAH features, little has been published on this feature and its companion near 5.7 μm .

The weak 5.25 and 5.7 μm PAH features do not correspond to fundamental vibrational frequencies (ν_i, ν_j, \dots), but are produced by overtone ($n \times \nu_i$), combination ($\nu_i + \nu_j$), and difference ($\nu_i - \nu_j$) bands of these fundamental vibrations (Allamandola et al. 1989a). For example, the strong CH out-of-plane (CH_{oop}) fundamental bending vibration (ν_{oop}) for solo hydrogens produces the well-known band at 11.2 μm (893 cm^{-1}). The overtone of this vibration, $2 \times \nu_{\text{oop}}$, is expected to produce a much weaker feature near 5.6 μm (1786 cm^{-1}) and is seen to contribute to the blue side of the broad 5.7 μm interstellar feature. Likewise, ν_{oop} could combine with

* Based on observations with *Infrared Space Observatory* (ISO), an ESA project with instruments funded by ESA member states (especially the PI countries: France, Germany, the Netherlands, and the United Kingdom) and with the participation of ISAS and NASA.

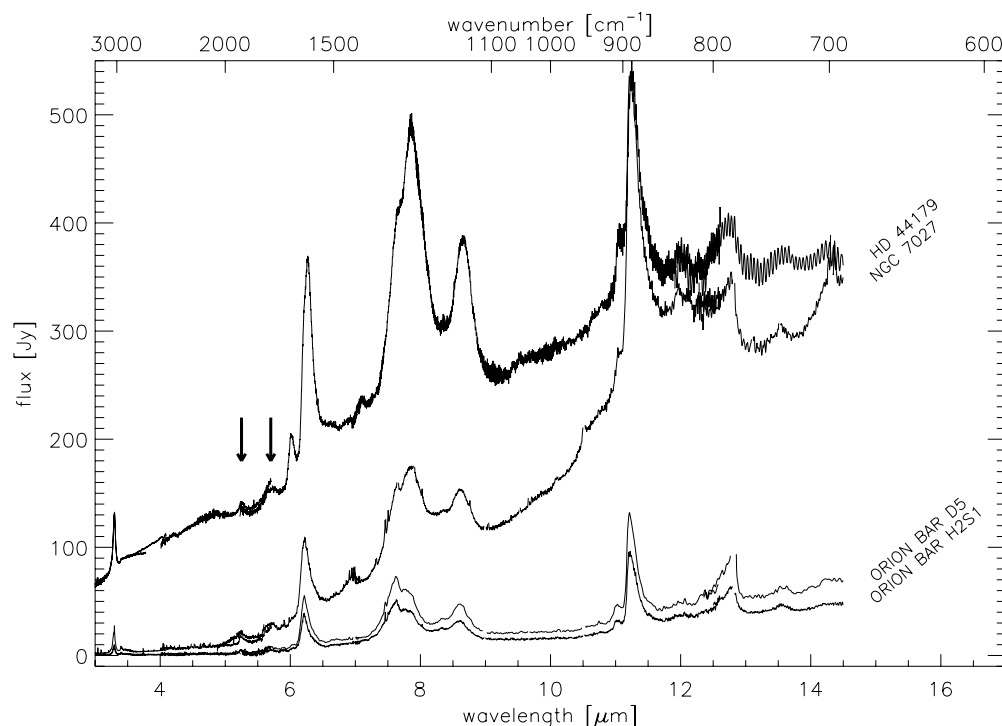


Figure 1. Extracted mid-IR spectra from 3 to 14.5 μm of the four sources considered here: HD 44179, NGC 7027, and the two positions along the Orion Bar. Spectra are shown at original resolution. For clarity the prominent atomic emission lines, e.g., at 5.61 ([Mg v]), 10.51 ([S iv]), and 12.81 ([Ne II]) μm , have been masked out. The arrows indicate the positions of the subtle 5.25 and 5.7 μm features.

a CC stretching vibration ($\nu_{\text{oop}} \pm \nu_{\text{CC}}$), resulting in other weak features.

Here, we present high-quality *Infrared Space Observatory* (ISO) Short Wavelength Spectrograph (SWS; de Graauw et al. 1996) spectra from four astronomical sources that show these features. The 5.25 and 5.7 μm bands are analyzed in terms of overtone, combination, and difference frequencies using experimental and theoretical PAH spectra. This paper is structured as follows. The astronomical observations are presented in Section 2, PAH spectroscopy is described in Section 3, astrophysical implications are drawn in Section 4, and a summary with conclusions is given in Section 5.

2. THE ASTRONOMICAL EMISSION FEATURES IN THE 5–6 μm (2000–1667 cm^{-1}) REGION

2.1. Observations

A sample of high-quality spectra from 15 sources, obtained by the SWS onboard ESA’s ISO, was investigated for PAH band emission in the 5–6 μm region. Of this set, the spectra from four objects that have sufficient signal-to-noise in this wavelength range permit an in-depth analysis.

The four sources considered here are HD 44179 (“Red Rectangle”), NGC 7027, and two positions on the Orion ionization ridge, H2S1 and D5. HD 44179 is the central binary star system of a bipolar planetary nebula, with one member being a post-AGB star. Both stars have a common circumstellar disk (e.g., Waelkens et al. 1996). NGC 7027 is a compact ($\sim 10^{16}$ cm) carbon-rich planetary nebula with a hot white dwarf at its center (Latter et al. 2000). The Orion Bar spectra probe the photon-dominated region that forms the interface between the bright H II region that is ionized by the Trapezium stars, and the Orion Molecular cloud; H2S1 and D5 are two positions within the

bar. Table 1 shows the journal of observations and the available astrometric data.

2.1.1. Data Reduction

The data have been obtained using the Astronomical Observing Template (AOT) 01 full scan mode at various speeds or the AOT 06 mode, providing spectra with a resolving power of 400–1600 ($\lambda/\Delta\lambda$). The data were processed with IA³, the SWS Interactive Analysis package, using calibration files and procedures equivalent with OLP version 6.0 or 10.1. A detailed account of the reduction can be found in Peeters et al. (2002). Figure 1 presents the raw extracted 2.38–45.2 μm ISO SWS spectra of the four sources at their original resolution. These data have not been defringed. The OSIA⁶ software package was drawn on to further reduce and analyze the data between 5 and 6 μm . Further reduction included bad data removal (e.g., glitches), edge truncation, splicing, and merging of detector bands. Uncertainties were estimated by comparing the up and down scans, yielding a measure for the noise. For HD 44179 a difference in absolute flux levels, not in shape, between the up and down scan was found. The up scan was scaled such that the mean of the up scan would match the mean of the down scan to compensate this. This can be done because our interest lies only in the uncertainty in the relative flux level, since those trace the reality of the shape of a feature. When required, the 5–6 μm spectra were binned to a constant resolution of 800 to facilitate one-to-one comparison. For Orion Bar position D5, this results in oversampling since the original data were obtained at a resolution of about 400. Table 2 presents a subset of the data reduction parameters and Figure 2 presents the fully reduced 5–6 μm ISO SWS spectra of the four sources at their original resolution.

⁶ OSIA is a joint development of the SWS consortium. Contributing institutes are SRON, MPE, KUL, and the ESA Astrophysics Division.

Table 1
Journal of Observations and Available Astrometric data

| Source | α (2000) (h m s) | δ (2000) ($^{\circ}$ ' ") | TDT | Obs. Mode (Speed) | Sp. Type | G_0 [Habing] | Object Type | Ref. |
|----------------|----------------------------|--------------------------------------|----------|----------------------|-------------------|-------------------|---------------|------|
| HD 44179 | 06 19 58.20 | -10 38 15.22 | 70201801 | 01 (4) | B8V | 5×10^6 | Post-AGB star | 1 |
| NGC 7027 | 21 07 01.70 | +42 14 09.10 | 55800537 | 06 | 2×10^5 K | 2×10^5 | PN | 1 |
| Orion Bar H2S1 | 05 35 20.31 | -05 25 19.99 | 69501806 | 01 (4) | O6 | 7×10^3 | H II region | 2 |
| Orion Bar D5 | 05 35 19.81 | -05 25 09.98 | 83101507 | 01 (2) | O6 | 5×10^4 | H II region | 3 |

References. (1) Beintema et al. 1996; (2) Verstraete et al. 2001; (3) Peeters et al. 2002.

Table 2
Data Reduction Parameters and Connected Wavelengths

| Source | OLP | Resolution | Continuum Points (μm) | Integration Bounds (μm) |
|----------------|--------------|------------------|---------------------------------------|---|
| HD 44179 | 10.1 | ~ 800 | 5.017;5.494;5.836;5.922 | 5.160;5.355;5.580;5.830 |
| NGC 7027 | 6.0/10.1 (1) | $\sim 1600/1000$ | 5.025;5.079;5.832;5.938 | 5.150;5.375;5.570;5.805 |
| Orion Bar H2S1 | 10.1 | ~ 800 | 5.102;5.415;5.825;5.969 | 5.170;5.374;5.590;5.820 |
| Orion Bar D5 | 10.1 | ~ 400 | 5.057;5.382;5.472;5.943 | 5.150;5.380;5.560;5.845 |

Notes. (1) The AOT 01 and AOT 06 data have been reduced with OLP version 6.0 and 10.1, respectively. The AOT 01 data are used in Figure 1 and the better quality AOT 06 data are presented in Figure 2 and used onward.

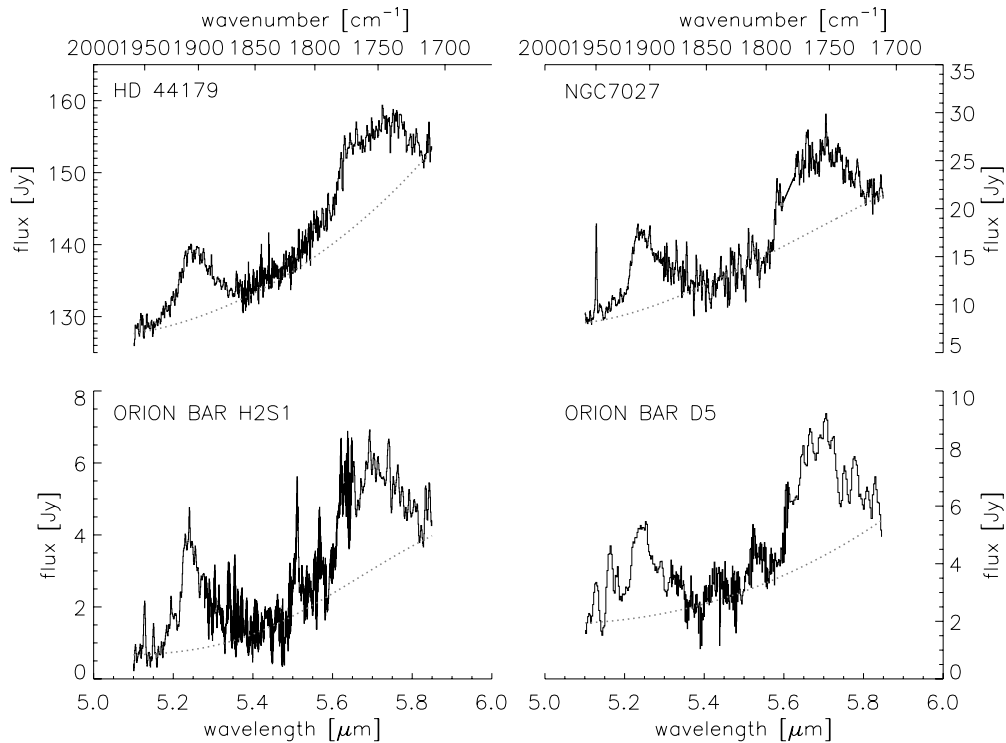


Figure 2. Fully reduced 5–6 μm spectra of the four objects considered. They are presented at original resolution. Also shown are the adopted continua.

2.2. Analysis

The spectra display a wealth of structure, including the familiar PAH bands at 3.3, 6.2, “7.7”, 8.6, 11.2, and 12.7 μm with their underlying plateaus and subfeatures. For clarity, several atomic emission lines have been masked out in Figure 1. Detailed analysis of the major features in the spectra have been published elsewhere (e.g., Hony et al. 2001; Peeters et al. 2002; van Diedenoven et al. 2004). Here, we focus on the PAH emission between 5 and 6 μm . As Figure 1 illustrates, the bands in this region are weak compared to the major features.

To isolate the PAH band profiles, a continuum is established for each object. The continua used apply only to the

5–6 μm region. Spline continua were constructed using connecting points between 5 and 6 μm , straddling the 5.25 and 5.7 μm features. The adopted continua are shown in Figure 2 and the connected wavelengths are listed in Table 2.

Atomic emission lines can also contribute to the emission in this region. For some of these objects, narrow lines at 5.128 (1950 cm^{-1} ; H I 6–10), 5.510 (1815 cm^{-1} ; H₂ 0 \rightarrow 0 S(7)), and 5.61 μm (1783 cm^{-1} ; [Mg v]) are present. Special care was taken to remove the 5.61 μm [Mg v] line in the spectrum of NGC 7027, where it is blended with the 5.75 μm PAH feature. The resulting continuum subtracted spectra are presented at equal resolution in Figure 3. Two broad bands, centered roughly at 5.25 and 5.7 μm , are clearly present in all objects and are quite

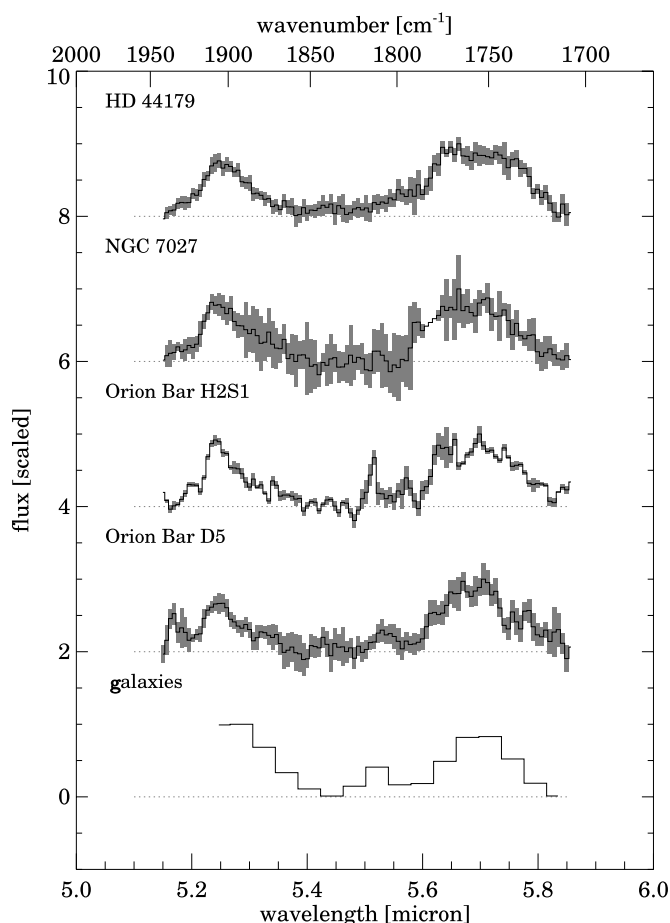


Figure 3. 5.25 and 5.7 μm PAH features in HD 44179, NGC 7027, and the Orion Bar: positions H2S1 and D5. All spectra are presented at $\lambda/\Delta\lambda = 800$ to aid comparison. These spectra were produced using the continuum and emission line corrections described in Section 2.2. To demonstrate the accessibility of the 5–6 μm region using *Spitzer*, the slightly redshifted average galaxy spectrum from Smith et al. (2007) is also presented, see Section 4 for a discussion.

similar within the uncertainty (systematic + noise). The 5.25 μm band is asymmetric and starts off near 5.15 μm (1942 cm^{-1}). For both positions in the Orion Bar it also seems to start off with a satellite feature, centered at about 5.2 μm (1923 cm^{-1}) and similar to those seen at 6.0 and 11.0 μm for the 6.2 and 11.2 μm bands, respectively. After a steep rise, the profile peaks at 5.25 μm (1905 cm^{-1}) and slowly declines to reach zero intensity near 5.4 μm (1852 cm^{-1}). This red wing resembles that seen for the 3.4, 6.2, and 11.2 μm features (Roche et al. 1996). Fitting the profiles at original resolution with a single Gaussian results in an FWHM of about $\sim 0.12 \pm 0.01\ \mu\text{m}$ ($\sim 42 \pm 6.5\text{ cm}^{-1}$).

The 5.7 μm feature is broader, and starts its rise near 5.55 μm (1802 cm^{-1}), just beyond the 5.51 μm (1815 cm^{-1}) $\text{H}_2\text{O} \rightarrow 0\text{ S}(7)$ line. The profile is unusual from about 5.65 μm (1770 cm^{-1}) to about 5.75 μm (1739 cm^{-1}), where the feature seems flat-topped and then drops to the continuum at 5.85 μm (1709 cm^{-1}). Some spectral structure is visible on the flat top, giving the impression of a blended double-peaked feature. Fitting the profile with a single Gaussian results in an FWHM of about $0.17 \pm 0.02\ \mu\text{m}$ ($\sim 51 \pm 5.6\text{ cm}^{-1}$).

After emission line removal the bands are integrated in the $\lambda - F_\lambda$ domain using a multiple Simpsons' rule, yielding band strengths in W m^{-2} . Uncertainties are calculated from the data. Table 3 summarizes these results and compares them with the band strengths of the dominant PAH bands.

3. PAH SPECTROSCOPY IN THE 5–6 μm (2000–1667 cm^{-1}) REGION

3.1. Experimental Studies

The matrix isolation IR spectroscopy techniques employed in this study have been described in detail previously (Hudgins & Allamandola 1995a, 1995b; Hudgins & Sandford 1998) and will be summarized here only briefly.

Matrix-isolated PAH samples were prepared by vapor co-deposition of the species of interest with an overabundance of argon onto a 14K CsI window suspended in a high-vacuum chamber ($p < 10^{-8}$ Torr). The samples were vaporized from heated Pyrex tubes while argon was admitted through an adjacent length of copper tubing, cooled by liquid nitrogen. The deposition temperatures, which are dependent on size and structure as well as the sources of the individual PAHs, are given in the references summarized in Table 1 of Mattioda et al. (2005).

Spectra from 1.7–20 μm ($6000\text{--}500\text{ cm}^{-1}$) were measured on either a Nicolet 740 or a Digi-Lab Excalibur FTS 4000 FTIR spectrometer using a KBr beam splitter and a liquid nitrogen cooled MCT detector. Each spectrum represents a co-addition of between 500 and 1024 scans at a resolution of 0.5 cm^{-1} . The number of scans was chosen to optimize both the signal-to-noise as well as time requirements for each experiment.

Figure 4 shows the 5–16.5 μm spectra of several matrix-isolated neutral PAHs. These spectra are typical of all spectra in the Ames collection of neutral PAH IR spectra and serve to illustrate that all PAHs have weak bands in the 5–6 μm region. For presentation purposes only, some of the data have been baseline corrected using the Digi-Lab data analysis software package. No further data reduction was necessary. All numerical values were obtained from the original (unaltered) data.

3.2. Theoretical

Previous work (e.g., Bauschlicher & Langhoff 1997; Bauschlicher 2002; Mattioda et al. 2003; Hudgins et al. 2005; Bauschlicher et al. 2008) have shown that density functional theory (DFT) calculations performed using the hybrid (Becke 1993) B3LYP (Stephens et al. 1994) approach in conjunction with the 4-31G basis set (Frisch et al. 1984) yield scaled harmonic frequencies that are in excellent agreement with results obtained from matrix isolation experiments. In this work, we expand our previous work by explicitly considering anharmonic effects (fundamental, overtone, combination, and difference bands), which are computed by doing numerical differentiation along the normal modes (Barone 2005) after the geometries are fully optimized and the harmonic frequencies are computed using analytic second derivatives. All of the DFT calculations are performed using the Gaussian 03 program system (Frisch et al. 2004). The vibrational modes are illustrated using Molekel⁷ (Portmann & Lüthi 2000).

As discussed previously, the DFT results differ systematically from experiment and hence need to be scaled (Bauschlicher & Langhoff 1997). The scaling factor depends on the level of theory (the correlation treatment and basis set), and it is common that CH stretches will have a different scaling factor from the other modes because of the large anharmonic effects for hydrogen stretching motions. In this work we use the small 4-31G set that has been used successfully in the significantly

⁷ MOLEKEL 4.3, P. Flükiger, H.P. Lüthi, S. Portmann, J. Weber, Swiss Center for Scientific Computing, Manno (Switzerland), 2000-2002.

Table 3The Integrated Band Strengths ($10^{-14} \text{ W m}^{-2}$) of the PAH Features Between 3 and $13 \mu\text{m}$ of HD 44179, NGC 7027, and the Orion Bar: Positions H2S1 and D5

| Source | 3.3 (1) (μm) | 5.25 (μm) | 5.75 (μm) | 6.2 (1) (μm) | 7.6 ^a (1) (μm) | 7.8 ^a (1) (μm) | 8.6 (1) (μm) | 11.2 (2) (μm) | 12.7 (μm) |
|----------------|------------------------------|---------------------------|---------------------------|------------------------------|---|---|------------------------------|-------------------------------|---------------------------|
| HD 44179 | 69 (1.4%) | 11 (1.5%) | 19 (1.3%) | 280 (10%) | 121 (10%) | 290 (10%) | 97 (10%) | 113 (10%) | 26 (5.4%) (3) |
| NGC 7027 | 24 (1.7%) | 9.1 (3.3%) | 13 (7.0%) | 95 (10%) | 40 (10%) | 63 (10%) | 28 (10%) | 130 (10%) | 36 (6.9%) (3) |
| Orion Bar H2S1 | 8.2 (1.6%) | 2.9 (1.6%) | 4.4 (1.7%) | 34 (10%) | 32 (10%) | 22 (10%) | 13 (10%) | 29 (10%) | 13 (10%) (2) |
| Orion Bar D5 | 11 (0.55%) | 3.7 (3.2%) | 6.1 (2.3%) | 12 (10%) | 40 (10%) | 36 (10%) | 24 (10%) | 40 (10%) | 17 (7.6%) |

Notes. Uncertainties are given in parentheses in percentages.

^a 7.6 and 7.8 μm bands have been separated using Gaussians.

References. (1) Peeters et al. 2002; (2) van Dienenhoven et al. 2004; (3) Hony et al. 2001.

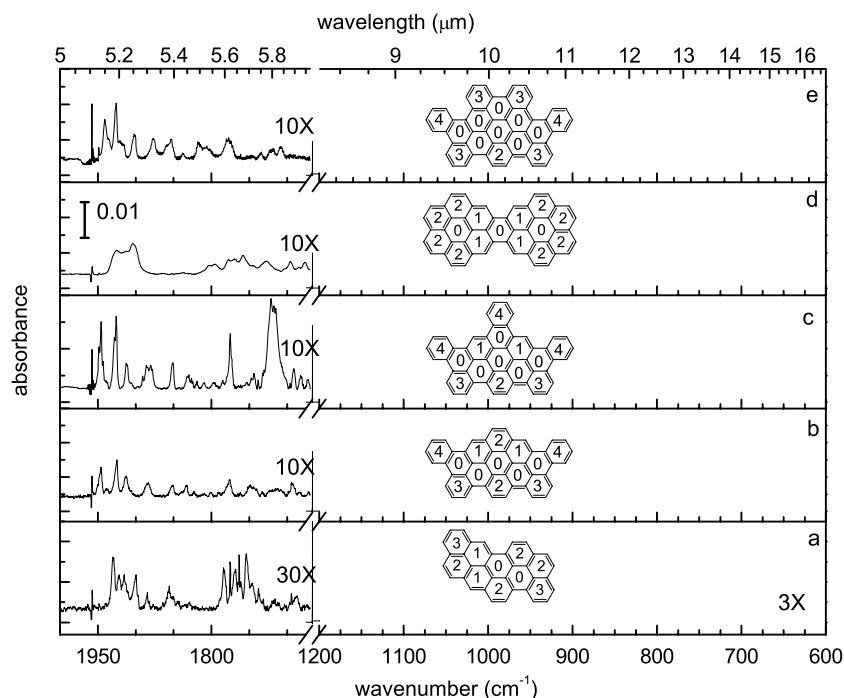


Figure 4. Matrix-isolated spectra for the CH_{Oop} region ($10\text{--}15 \mu\text{m}$) as well as the overtone and combination band region ($5\text{--}6 \mu\text{m}$) for various neutral PAHs containing solo, duo, trio, and quartet hydrogens. The number of adjacent hydrogen atoms per ring are indicated in the structure.

larger and more precise, but also more time consuming, 6-311G** basis set (Frisch et al. 1984). The larger 6-311G** basis set was used for naphthalene (C_{10}H_8) because of its small size. The results from the large basis set allow us to calibrate the smaller basis set that is required for the larger molecules. We use the matrix isolation experiments of Hudgins et al. (1994) for the calibration of neutral naphthalene. While gas-phase data exists, we use the matrix isolation experiments to allow a direct comparison between our experiments and our computed values. In addition, it has been shown by, e.g., Oomens et al. (2000) and Allamandola & Hudgins (2003) that there is a very good agreement between the gas phase and matrix isolation results.

Comparison of the computed fundamental frequencies of neutral naphthalene, using the 6-311G** basis set, shows that a scale factor of 0.998 brings the computed non-CH stretching modes (i.e., all the bands excluding the CH stretching modes) into good agreement with experiment. This comparison shows an average absolute error of 2.6 cm^{-1} and a maximum absolute error of 9 cm^{-1} between experiment and theory. A scale factor of 1.005 brings the computed CH stretching modes into good agreement (a maximum error of 7 cm^{-1}) with experiment. This accordance with experiment is consistent with recent work by Cane et al. (2007), who find good agreement between theory

and experiment using a hybrid functional and a large basis set (B971/TZ2P). For the smaller 4-31G basis set we find a scale factor of 0.976 for the non-CH stretching fundamentals and 1.007 for the CH stretching fundamentals. The maximum absolute error in the non-CH stretching modes is 19 cm^{-1} , a value greater than that when using the larger basis set, but still sufficiently small to allow a qualitative understanding using the small basis set. It is interesting to note that two scale factors are needed for the 4-31G fundamentals while only one scale factor is needed for the 4-31G harmonics.

Since the scale factors for the 6-311G** basis set are very close to 1, we do not use any scaling for the overtone, combination, or difference bands. For the 4-31G basis set, the overtone and combination bands are scaled by 0.976, the scale factor for the non-CH stretching modes, because the CH stretches are not involved in the overtone or combination bands of interest. For the difference bands, the non-CH stretching fundamentals are scaled by 0.976, while the CH stretching fundamentals are scaled by 1.007. While the level of theory used is expected to yield accurate band positions for the overtones, combination, and difference bands, the current version of Gaussian does not determine intensities for these bands. However, as discussed in Section 3.3.2, selection rules allow the exclusion of some

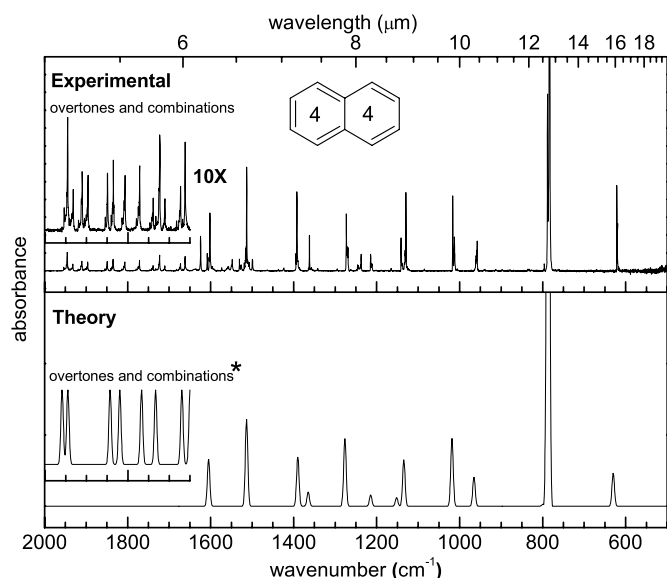


Figure 5. Comparison between the B3LYP-level calculated and experimentally obtained spectra of naphthalene from 5 to 19 μm , showing their outstanding agreement for fundamentals. The agreement for the overtone and combination bands is reasonable.

* **Note** that the theoretical results for the overtone and combination bands do not calculate intensities. Therefore, the bands were derived from fundamentals with an intensity greater than 10 km mole^{-1} and given the same intensity to allow for comparison with the experimental frequencies.

combination and difference bands as possible contributors to the observed features. In addition to excluding some bands, we speculate on which allowed bands will be the strongest. In the harmonic approximation, the second derivative of the dipole moment is responsible for the intensity of the first overtone, but in the real world, anharmonicity means that the overtones will have some contributions from the first derivative. This implies that the strongest overtone, combination, and difference bands will commonly involve the strongest fundamentals.

Figure 5 compares the 5–19 μm ($2000\text{--}530 \text{ cm}^{-1}$) spectrum of neutral naphthalene computed using DFT at the B3LYP level to the spectrum of matrix-isolated neutral naphthalene (C_{10}H_8) from Hudgins et al. (1994). This figure demonstrates the excellent agreement between the theoretically computed and experimentally measured mid-IR spectrum for fundamentals and the reasonable agreement in the positions of the calculated overtone and combination bands. Note that difference bands only arise from emission processes and are thus not found in the experimental spectra.

3.3. The Origin of the PAH Bands in the 5–6 μm ($2000\text{--}1667 \text{ cm}^{-1}$) Range

The experimental spectra presented in Figure 4 illustrate what has long been known—PAHs show weak spectral structure in the 5–6 μm ($2000\text{--}1667 \text{ cm}^{-1}$) region. This structure has been attributed to overtones and combination bands based on spectroscopic studies of small aromatic molecules (Young et al. 1951). This work is summarized below, followed by a detailed analysis of the PAH vibrations that produce bands in the 5–6 μm region for large PAHs, species comparable in size to the astronomical PAHs.

Young et al. (1951) present some examples of the distinctive band patterns in the 5–6 μm region produced by different substituted benzenes. The different substitution patterns force different H adjacencies and this has been found to determine

the characteristic band patterns in this region. This behavior strongly suggests that fundamental vibrations associated with hydrogen are the primary carriers of this spectroscopic structure, but these different substitution patterns could also induce IR activity in transitions involving CC vibrations. The central role of hydrogen in producing these features is confirmed when one compares the 5–6 μm region of the spectra of normal PAHs (C_xH_y) with the same region in the spectra of fully deuterated PAHs (PADs; C_xD_y). The absence of any activity in the 5–6 μm region of the deuterated PAH spectra shows that hydrogen is essential in producing these features. The band patterns in the 5–6 μm region reflect hydrogen adjacency because, as discussed below, they involve strong CH vibrations whose fundamental frequencies are determined by their adjacency class.

3.3.1. Experimental

The 5–6 μm region of the astronomical emission spectrum was initially thought to be dominated by simple combinations and overtones of the fundamental CH_{oop} modes (Bellamy 1960). Thus our analysis begins by separating out the contributions of the CH_{oop} modes. The CH_{oop} region, which falls between 10.5 and 15 μm , includes contributions of the solo (nonadjacent hydrogens), duo (doubly adjacent hydrogens), trio (triply adjacent hydrogens), and quartet (quadruply adjacent hydrogens) hydrogens present on a PAH (e.g., Hudgins & Allamandola 1999). Each of these types of vibrations falls within specific wavelength regions. Given the segregation of the CH_{oop} vibrations in PAH spectra, one would expect combination modes arising from these fundamental vibrations to be similarly grouped (i.e., quartets furthest to the red and solos furthest to the blue), if the various CH_{oop} modes combined with the same vibrational modes. To better understand this region, we have analyzed the spectra of over 35 neutral PAHs of various sizes and structures and have found that this is not necessarily the case. While several features between 5 and 6 μm appear to be the result of solo, duo, trio, and quartet hydrogens, their order does not follow that which is observed in the CH_{oop} region.

The CH_{oop} spectra of several matrix-isolated PAHs are shown in conjunction with their respective overtone and combination regions in Figure 4. As one can easily see, the CH_{oop} region varies considerably with respect to the various PAH structures, reflecting the variability in the solo, duo, trio, and quartet hydrogens from one PAH to the next. Likewise there is considerable variability in the overtone and combination region (5.1–5.8 μm region). Close inspection of Figure 4 reveals that molecules b, c, and e contain a large set of bands spanning the full wavelength region, while molecules a and d have a pronounced break in the overtone and combination bands between the 5.25 and 5.7 μm regions. The major structural difference in these PAHs is the presence of quartet hydrogens in molecules b, c, and e. The presence of quartet hydrogens in a PAH molecule produces a complex of bands spanning the entire 5 and 6 μm region, making them unsuitable for being responsible for the astronomical 5.25 and 5.7 μm features.

Ignoring, for the moment, the fundamental vibrational modes as carriers of the overtone and combination bands, several additional interesting trends appear in the 5–6 μm region that can be linked to the PAH structure. The PAH spectra presented in Figure 6 will assist in identifying these trends. The positions of the astronomical 5.25 and 5.7 μm have been indicated by the shaded areas, with, on both sides, an uncertainty of $\sim 10 \text{ cm}^{-1}$ to account for cold absorption versus hot emission

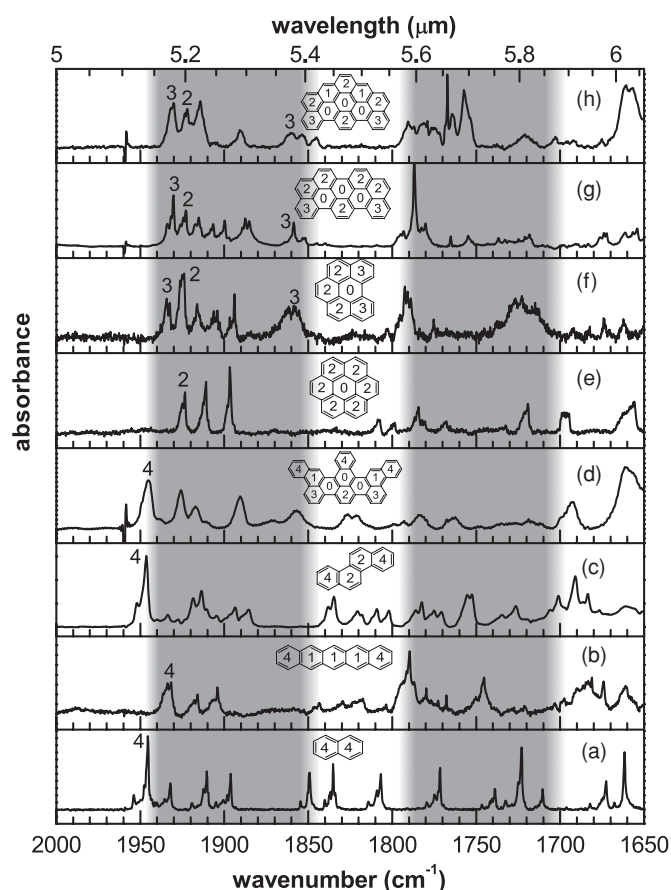


Figure 6. Matrix-isolated spectra of (a) naphthalene, (b) pentacene, (c) chrysene, (d) large, uncondensed PAH containing solo, duo, trio, and quartet hydrogens, (e) coronene, (f) benzo[ghi]perylene, (g) large PAH containing only duo and trio hydrogens, and (h) large PAH containing duo, trio, and solo hydrogens. Bands identified as involving quartet hydrogens are labeled with a “4,” trio hydrogens a “3,” and duos a “2.” The shaded areas show the band positions of the 5.25 and 5.7 μm astronomical features.

(Joblin et al. 1995). The first trend to note is that all the matrix-isolated PAHs in Figure 6, along with all the PAHs investigated by this lab to date, exhibit bands in the 5.25 and 5.7 μm regions. The quartet containing PAHs, in addition to exhibiting bands in undesirable positions, also tend to have bands to the blue and red of the positions occupied by the 5.25 and 5.7 μm astronomical features. For instance, in Figure 6(a) the bands extend further to the blue of the 5.25 μm area than the bands visible in the PAHs that are shown in Figures 6(e), 6(f), 6(g), and 6(h), which contain only solo, duo, and trio hydrogens. Furthermore, quartets that are part of a “bay” region in PAHs, such as found in Figures 6(c) or 6(d), tend to produce bands at wavelengths shorter than those of less hindered quartets, such as those shown in Figures 6(a) and 6(b). Typically, the bay region quartets result in a band around 5.128 μm (1950 cm^{-1}) versus the 5.14 μm (1940 cm^{-1}) position of the less hindered quartet. Thus PAHs containing quartet hydrogens will exhibit bands outside the area occupied by the 5.25 and 5.7 μm astronomical features.

Additional analysis reveals that PAHs with duo hydrogens tend to exhibit a band around 5.19 μm (1925 cm^{-1}), see Figure 6(e). The presence of trio hydrogens, in addition to duos, tends to produce another feature to the blue of the duo band around $\sim 5.18 \mu\text{m}$ (1930 cm^{-1}). This is clearly illustrated in the spectra shown in Figures 6(e), 6(f), 6(g) and 6(h), where the trios, labeled as “3,” in Figures 6(f), 6(g), and 6(h) produce a band further to the blue of the duo band, labeled as “2,” in

Figure 6(e). However, in the absence of duo hydrogens, the trios produce a single feature near the position of the lone duo hydrogens. Finally, the presence of hydrogen trios also tends to produce a feature just to the red of the 5.25 μm band area ($\sim 5.39 \mu\text{m}$ or 1855 cm^{-1}). This feature is readily observed (labeled with a “3”) in the matrix-isolated spectrum shown in Figure 6(f), as well as in the spectra shown in Figures 6(g) and 6(h). Although all of the PAHs with trio hydrogens exhibited this feature, the intensity of this band depends on the specific PAH structure. Thus, PAHs containing only duo and trio hydrogens match the 5.25 μm astronomical feature well, but PAHs containing trio hydrogens match only marginally due the presence of a band around 5.39 μm . This implies a limited concentration of PAHs containing trio hydrogens in astronomical objects.

The matrix-isolated PAH absorption spectra in the 5.7 μm astronomical band region, running from ~ 5.5 to 5.8 μm , exhibit considerably more variability than the 5.25 μm region. Just as in the 5.25 μm region, every PAH investigated shows bands in the 5.7 μm region. However, there seems to be a greater degree of segregation concerning the absorptions in this region. While the presence of quartet hydrogens produce bands in the 5.7 μm region, their presence also tends to produce bands to the blue and red of the region. This is exemplified in the spectra shown in Figures 6(a), 6(b), and 6(c). Although PAHs containing only duo and trio hydrogens match the 5.7 μm feature very well, their bands tend to cluster around 5.6 μm (1780 cm^{-1}), whereas the presence of solos extends this structure toward 5.8 μm (1724 cm^{-1}). This is beautifully illustrated in the PAH spectra shown in Figures 6(f), 6(g), and 6(h). The PAHs producing the spectra in Figures 6(e) and 6(g) contain only doubly and triply adjacent hydrogens, while the top spectrum is of a similar PAH but containing solo hydrogens. As is easily seen in Figure 6, although PAHs containing duo and trio hydrogens can contribute to the 5.7 μm astronomical feature, solo hydrogens are required to match the full 5.7 μm feature.

In addition to possessing bands to the blue of the 5.25 μm feature and bands to the blue and red of the 5.7 μm feature, PAHs containing quartet hydrogens exhibit an additional trait which prohibit them from effectively matching the 5.25 and 5.7 μm astronomical regions. This concerns the region between the 5.25 and 5.7 μm astronomical features. As shown in Figures 6(a), 6(c), and 6(d), PAHs containing quartets exhibit more intense activity in the area *between* the 5.25 and 5.7 μm features than PAHs containing only solos, duos, and trios. In fact, as all the spectra in Figures 4 and 6 reveal, PAHs containing quartets seem to exhibit a continuum of bands throughout the region that includes the 5.25 and 5.7 μm features. This is exemplified in the PAH spectrum shown in Figure 6(d). Although it is a fairly large PAH, its open structure contains solo, duo, trio, and quartet hydrogens. Likewise its spectrum exhibits a continuum of bands throughout the region containing the 5.25 and 5.7 μm features.

Two final notes should be made regarding PAH structure and the overtone and combination region. First, *not all of the experimentally measured features in this region can be traced back to the strongest solo, duo, trio, and quartet hydrogen bands.* This precludes a one-to-one assignment with the theoretical results for all the bands presented in the next section. This region also contains bands around 1903 cm^{-1} (5.25 μm ; $\pm 5 \text{ cm}^{-1}$) and 1915 cm^{-1} (5.22 μm ; $\pm 5 \text{ cm}^{-1}$), which appear in the PAH spectra collected regardless of structure. In a few instances, either the 1903 or 1915 cm^{-1} band will appear by itself, but in most instances both bands are present. Due

to the appearance of at least one of these bands in all of the PAH spectra, we were unable to associate them with a particular structural feature. However, the absence of any bands between 5 and 6 μm in fully deuterated PAH spectra indicates that hydrogen motion is involved, obviously through CH in-plane (CH_{ip}) modes. Second, while difference bands only arise from emission processes and are thus not found in the absorption spectra presented here, they will likely contribute to the astronomically observed features.

In summary, the experimental evidence suggests that the astronomical 5.25 and 5.7 μm features can be accommodated by the overtone and combination bands resulting from PAHs containing trio, duo, and solo hydrogens. The presence of a band around 5.39 μm in PAHs containing trio hydrogens implies a limit of the concentration of this particular PAH structure in the astronomical PAH population. The presence of quartet hydrogens produces undesirable features in the spectrum. The 5.7 μm region exhibits a greater variability in structure than the 5.25 μm . This greater variability is the result of PAHs with only duo and trio hydrogens producing absorption features which cluster on the blue side of the 5.7 μm region, whereas the presence of solo hydrogens is necessary to produce features toward the red side of this region. Such variability could be utilized as a tracer of PAH structures in astronomical environments.

3.3.2. Theoretical Studies

Computational spectra permit an extensive analysis of the nature of the transitions that produce features in the 5–6 μm region, including difference bands which are inaccessible through experimental absorption spectroscopy. Figure 5 compares the spectrum of neutral naphthalene computed using DFT at the B3LYP level to the spectrum of matrix-isolated neutral naphthalene (C_{10}H_8). This figure illustrates two important points. First, it demonstrates the excellent agreement between the experimentally measured and theoretically computed *fundamental* transitions that produce the mid-IR spectrum of naphthalene. Second, this level of theory does not predict any fundamental PAH vibrations between 5 and 6 μm , adding further support of their assignment to combination and overtone types of bands.

We now consider neutral naphthalene using the 6-311G** basis set. The results are summarized in the top two sections of Table 4. There are no overtones between 5 and 6 μm that are derived from fundamentals with intensity greater than 10 km mole⁻¹. Therefore, we conclude that overtones are not responsible for the bands between 5 and 6 μm in the spectrum of naphthalene. However, naphthalene is a special case since it has only quartet hydrogens and, as shown in Table 5 for coronene, overtones can produce important bands in this region. We now consider combination and difference bands instead of overtones. Because of the high symmetry in naphthalene, dipole-allowed combination and difference bands can only arise from a forbidden mode interacting with an allowed mode. In addition to this rigorous selection rule, we presume that the stronger bands will result from combinations and differences in which the allowed band is intense (Section 3.2). The combination and difference bands of the most interest in the 5–6 μm range are also summarized in Table 4. All of the computed combination bands in neutral naphthalene involve the strong CH_{oop} bending mode (B_{3u}) at 12.703 μm . The vibration producing this strong band couples with forbidden in-plane and out-of-plane CH bending vibrations to produce the combination bands. The fundamental modes are visualized in Figure 7. Hence, since the only strong

bands in neutral naphthalene are the CH_{oop} bend and the CH stretch, and the higher frequency CH stretch cannot contribute to the combination bands in the 5–6 μm region, the only bands in the correct region that can couple with the strong B_{3u} CH_{oop} band to produce features in the correct region are other CH bends. Given that difference bands will involve a higher-frequency mode and that the only strong, allowed higher frequency fundamental is the allowed CH stretch, all difference modes falling between 5 and 6 μm must involve coupling of the allowed CH stretch with *forbidden* CH_{ip} bending vibrations.

The results for the 4-31G basis set are rather similar to those of the larger basis set and are presented in the lower section of Table 4. The combination bands are in somewhat better agreement than the difference bands, but overall the small basis set results are in good agreement with those from the larger basis set. Therefore, we also computed the overtone, combination, and difference bands in neutral coronene with the 4-31G basis set; these results are given in Table 5. While coronene has D6h symmetry, we use D2h symmetry labels to facilitate comparison with naphthalene. In this way, the similarities between the vibrational symmetries are more readily apparent. It is important to note that coronene has duo hydrogens, not quartet hydrogens as in naphthalene. The CH_{oop} band in coronene falls at 11.538 μm (867 cm⁻¹), whereas in naphthalene it is at 12.677 μm (789 cm⁻¹). Consequently, coronene has an overtone band in the 5–6 μm region derived from this strong fundamental. Extrapolating to other PAHs, on the basis of typical band positions for CH_{oop} bends, it is clear that PAHs containing solo and duo hydrogens will have overtone bands in the 5–6 μm region, a result consistent with the experimental conclusions in Section 3.3.1. The second point to note from the computed coronene tabulation is that all of the combination bands involve CH_{ip} and CH_{oop} bending modes coupled to the one strong out-of-plane mode. As for naphthalene, the difference bands arise from a coupling of a strong CH stretch with forbidden CH_{ip} bending modes.

The naphthalene cation was also studied using the 6-311G** basis set and the results are given in the middle section of Table 4, with visualizations of the modes in Figure 8. In contrast with neutral naphthalene, the first point to note is that, since ionization increases the intrinsic strength of many bands, the cation has several strong bands that can contribute to combination bands. For naphthalene, the contribution bands are mostly CH_{ip} and CH_{oop} bending in character, but some begin to have contributions from modes with CC stretching and bending character. For example, the bands at 23 and 21 μm (435 and 476 cm⁻¹) have significant CC contributions to the mode. As the cation grows in size and the number of low-frequency modes increases, we presume that the character of the vibrations that produce combination bands in the cation could become even more diverse. The second difference between the neutral and cation forms is that the cation difference bands involve an allowed CH bend and forbidden CH stretches. That is, the same strong CH_{ip} bend that contributes to the combination bands is also the allowed band contributing to the difference bands.

Comparing the position of the computed combination bands with the frequencies of the two fundamentals that comprise the bands shows only a small shift (2.6 cm⁻¹) for the region of interest. This, coupled with the spectroscopic property that difference bands fall at ($\nu_i - \nu_j$) without any shift (Herzberg 1945), permits using scaled harmonic frequencies from larger PAHs as a guide in assessing the fundamental bands that can contribute to the observed overtone, difference, and combination

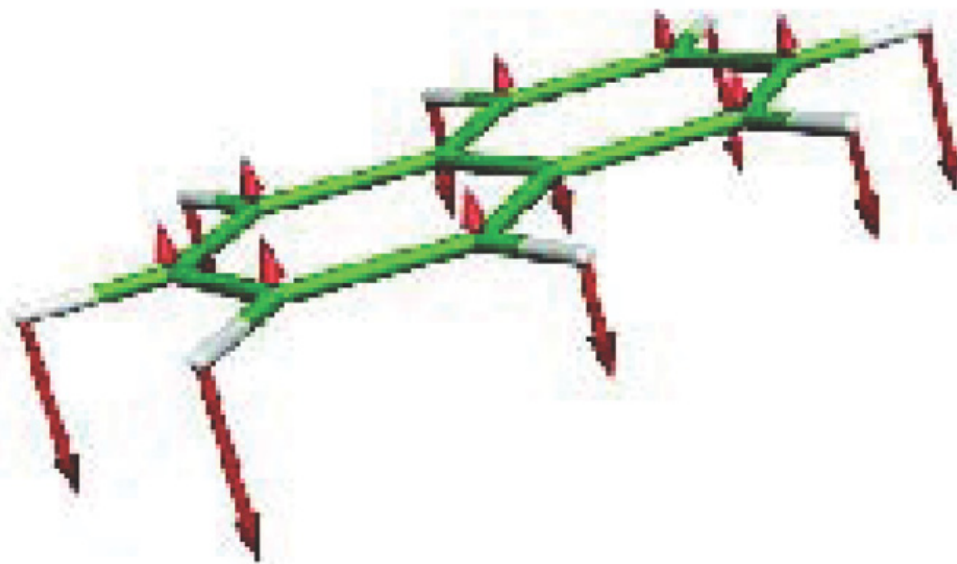


Figure 7. Example of one fundamental CH vibrational mode illustrative of the combination and difference bands of neutral naphthalene listed in Table 4. The carbon skeleton is depicted in green, the hydrogen atoms in white, and the vibrational motion of the molecule is indicated by the red vector arrows. Visualizations for all modes are available in the electronic edition of the Journal.

(An extended version of this figure is available in the online journal.)

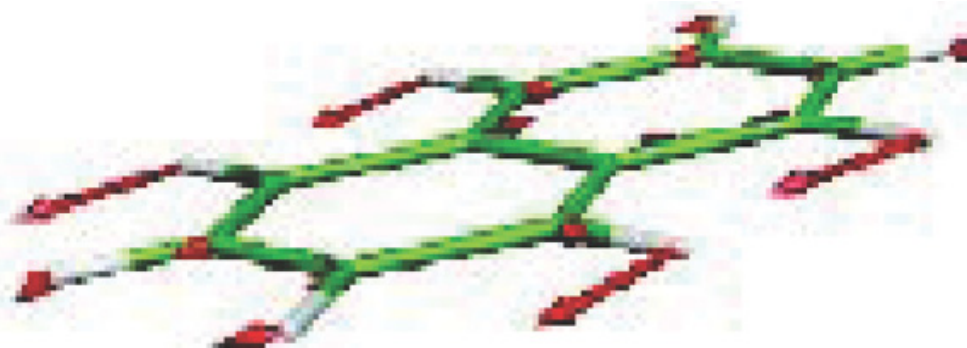


Figure 8. Example of one fundamental CH vibrational mode illustrative of the combination and difference bands of the naphthalene cation listed in 4. The carbon skeleton is depicted in green, the hydrogen atoms in white, and the vibrational motion of the molecule is indicated by the red vector arrows. Visualizations for all modes are available in the electronic edition of the Journal.

(An extended version of this figure is available in the online journal.)

bands. Considering the modes in three very large regular PAHs, $C_{110}H_{26}$, $C_{112}H_{26}$, and $C_{130}H_{28}$, we find that the cation, neutral, and anion forms of all three molecules should each have strong overtones near $5.4\text{--}5.6\ \mu\text{m}$ ($1818\ \text{cm}^{-1}$). Considering that we are computing the overtone as twice the scaled harmonics, the $5.4\text{--}5.6\ \mu\text{m}$ bands are consistent with the astronomical $5.7\ \mu\text{m}$ feature that arises from overtones of large symmetric PAHs. All three charge states of all three molecules have many possible combination and difference bands in the $5\text{--}6\ \mu\text{m}$ region. For the neutral combination bands, the strongest allowed components are CH_{oop} bends, the same as found for the smaller molecules. However, it is interesting to note that there are combination bands in this region that are derived from an allowed CH_{ip} bend with a forbidden CH_{oop} bend and an allowed CC stretch with a forbidden drum head mode; the intensity of the allowed CH_{ip} bend and CC stretch is about 25% of the CH_{oop} bend. For anions and cations, the intensity of the CH_{ip} and CC stretch can exceed the strongest CH_{oop} bending vibration. For large PAH cations, the CH-stretch intensity can be sizable, therefore difference bands in the $5\text{--}6\ \mu\text{m}$ region can arise from an allowed CH stretch as well as from an allowed CH bend. Overall, the

anion spectra in the $5\text{--}6\ \mu\text{m}$ region is more similar to that of the cation than that of the neutral.

Summing up, the computational work supports the idea that PAH neutrals, cations, and anions have overtones arising from CH_{oop} bends of solo and duo hydrogens that fall in the $5\text{--}6\ \mu\text{m}$, as do combination bands arising from in- and out-of-plane CH bends. In addition to the combination bands, difference bands, involving CH stretches and CH bends, can also fall in this region. Since there are more strong bands in the cations and anions than in the neutrals, more combination bands arise. It is likely that in large PAH ions, not all of the combination bands arise from only CH_{ip} and CC_{oop} bends.

For now, our theoretical study is limited by the inability to compute intensities. Without intensities the theory is not able to make a one-to-one comparison with the laboratory spectra and it is impossible to definitively establish which combination and difference bands could contribute to the astronomical spectrum. However, the calculations support the idea that neutrals, cations, and anions of large PAHs can all contribute to the observed features. Specifically, (1) the CH_{oop} solo and duo hydrogens lead to an overtone in the region of interest, (2) combination bands

Table 4
The Computed Combination and Difference Bands for Naphthalene

| Forbidden Transition | | | | Allowed Transition | | | |
|--|---------------------------------|-----------------|--------|---------------------------------|-----------------|--------|--|
| Wavelength (μm)/(cm^{-1}) | Wavelength (μm) | Symmetry | Figure | Wavelength (μm) | Symmetry | Figure | Intensity (Km mole^{-1}) |
| Naphthalene 6-311G** neutral | | | | | | | |
| Combination | | | | | | | |
| 5.989/1670 | 11.330 | B _{2g} | b | | | | |
| 5.770/1733 | 10.570 | B _{1g} | c | | | | |
| 5.660/1767 | 10.194 | B _{2g} | d | 12.703 | B _{3u} | a | 114.1 |
| 5.496/1820 | 9.680 | A _g | e | | | | |
| 5.104/1959 | 8.537 | A _g | f | | | | |
| Difference | | | | | | | |
| 5.977/1673 | 7.324 | A _g | h | | | | |
| 5.583/1791 | 8.017 | B _{3g} | i | 3.291 | B _{1u} | g | 64.1 |
| 5.356/1867 | 8.537 | A _g | f | | | | |
| 5.309/1884 | 8.660 | B _{3g} | j | | | | |
| 5.894/1679 | 7.324 | A _g | h | | | | |
| 5.510/1815 | 8.017 | B _{3g} | i | 3.266 | B _{2u} | k | 49.1 |
| 5.289/1891 | 8.537 | A _g | f | | | | |
| 5.243/1907 | 8.660 | B _{3g} | j | | | | |
| Naphthalene 6-311G** cation | | | | | | | |
| Combination | | | | | | | |
| 5.948/1681 | 21.365 | B _{3g} | d | 8.239 | B _{2u} | a | 218.8 |
| 5.896/1696 | 10.751 | B _{2g} | e | 13.047 | B _{3u} | b | 105.7 |
| 5.804/1723 | 19.626 | A _g | f | 8.239 | B _{2u} | a | 218.8 |
| 5.779/1730 | 10.366 | B _{1g} | g | 13.047 | B _{3u} | b | 105.7 |
| 5.610/1783 | 9.826 | B _{2g} | h | 13.047 | B _{3u} | b | 105.7 |
| 5.511/1815 | 9.541 | A _g | i | 13.047 | B _{3u} | b | 105.7 |
| 5.129/1950 | 23.198 | B _{2g} | j | 6.569 | B _{1u} | c | 87.41 |
| 5.116/1955 | 13.499 | B _{1g} | k | 8.239 | B _{2u} | a | 218.8 |
| 5.110/1957 | 8.410 | A _g | l | 13.047 | B _{3u} | b | 105.7 |
| 5.063/1975 | 13.131 | A _g | m | 8.239 | B _{2u} | a | 218.8 |
| 5.027/1989 | 21.365 | B _{3g} | d | 6.569 | B _{1u} | c | 87.4 |
| Difference | | | | | | | |
| 5.415/1847 | 3.267 | A _g | n | | | | |
| 5.410/1848 | 3.266 | B _{3g} | o | 8.239 | B _{2u} | a | 218.8 |
| 5.371/1862 | 3.252 | B _{3g} | p | | | | |
| Naphthalene 4-31G neutral | | | | | | | |
| Combination | | | | | | | |
| 5.977/1673 | 11.296 | B _{2g} | ... | | | | |
| 5.776/1731 | 10.600 | B _{1g} | ... | | | | |
| 5.637/1774 | 10.134 | B _{2g} | ... | 12.677 | B _{3u} | ... | 111.2 |
| 5.521/1811 | 9.768 | A _g | ... | | | | |
| 5.078/1969 | 8.479 | A _g | ... | | | | |
| Difference | | | | | | | |
| 5.796/1725 | 7.386 | A _g | ... | | | | |
| 5.484/1823 | 7.965 | B _{3g} | ... | 3.248 | B _{1u} | ... | 78.1 |
| 5.264/1900 | 8.479 | A _g | ... | | | | |
| 5.212/1919 | 8.618 | B _{3g} | ... | | | | |
| 5.738/1743 | 7.386 | A _g | ... | | | | |
| 5.431/1841 | 7.965 | B _{3g} | ... | 3.229 | B _{2u} | ... | 71.4 |
| 5.216/1917 | 8.479 | A _g | ... | | | | |
| 5.165/1936 | 8.618 | B _{3g} | ... | | | | |

Notes. Band positions determined using the 6-311G** basis set are compared to those determined using the 4-31G basis set. The forbidden and allowed transitions that produce each band are given. Visualization of the fundamental vibrations producing the combination and difference bands indicated here in Columns 4 and 7 are shown in Figures 7 and 8.

arising from in- and out-of-plane CH bends can also contribute to the observed bands, and (3) difference bands involving CH stretches and CH bends can also contribute to the observed bands.

4. ASTROPHYSICAL CONSIDERATIONS

First, we consider the 5.25 μm band. The few earlier studies of this band focused on its general attributes. Allamandola

Table 5

The Computed Overtone, Combination and Difference Bands for Neutral Coronene Computed Using the 4-31G Basis Set

| Forbidden Transition | | | Allowed Transition | | |
|--|---------------------------------|----------|---------------------------------|----------|--|
| Wavelength (μm)/(cm^{-1}) | Wavelength (μm) | Symmetry | Wavelength (μm) | Symmetry | Intensity (Km mole^{-1}) |
| Overtone | | | | | |
| 5.770/1733 | | | 11.538 | B_{3u} | 175.6 |
| Combination | | | | | |
| 5.857/1707 | 11.890 | B_{1g} | | | |
| 5.723/1747 | 11.349 | B_{2g} | | | |
| 5.640/1773 | 11.041 | B_{2g} | | | |
| 5.475/1826 | 10.409 | B_{1g} | 11.538 | B_{3u} | 175.6 |
| 5.470/1828 | 10.394 | B_{2g} | | | |
| 5.432/1841 | 10.252 | B_{2g} | | | |
| 5.383/1858 | 10.091 | A_g | | | |
| 5.281/1894 | 9.739 | A_g | | | |
| Difference | | | | | |
| 5.917/1690 | 7.206 | B_{3g} | | | |
| 5.916/1690 | 7.207 | A_g | | | |
| 5.732/1745 | 7.501 | A_g | | | |
| 5.460/1832 | 8.024 | B_{3g} | | | |
| 5.421/1845 | 8.110 | A_g | 3.249 | B_{1u} | 140.3 |
| 5.399/1852 | 8.159 | B_{3g} | | | |
| 5.396/1853 | 8.166 | A_g | | | |
| 5.253/1904 | 8.517 | A_g | | | |
| 5.252/1904 | 8.519 | B_{3g} | | | |
| 5.989/1670 | 7.024 | B_{3g} | | | |
| 5.987/1670 | 7.026 | A_g | | | |
| 5.863/1706 | 7.206 | B_{3g} | | | |
| 5.862/1706 | 7.207 | A_g | | | |
| 5.681/1760 | 7.501 | A_g | | | |
| 5.414/1847 | 8.024 | B_{3g} | 3.233 | B_{2u} | 139.4 |
| 5.375/1860 | 8.110 | A_g | | | |
| 5.354/1868 | 8.159 | B_{3g} | | | |
| 5.351/1869 | 8.166 | A_g | | | |
| 5.210/1919 | 8.517 | A_g | | | |
| 5.209/1920 | 8.519 | B_{3g} | | | |

Note. The forbidden and allowed transitions producing each band are given. et al. (1989b) and Roche et al. (1996) attributed this feature to overtones and combinations involving the lower lying CH_{oop} bending modes. For three of the four objects considered here, the 5.25 μm emission band has an FWHM of 0.11 μm (40 cm^{-1}). It may be slightly broader in NGC 7027 (0.14 μm , 50 cm^{-1}), but the lower signal to noise in this object makes this value less reliable. Roche et al. (1996) noted the striking similarity between the profiles of the 5.25 μm band and that of the 3.4, 6.2, and 11.2 μm bands. This comparison is revisited in Figure 9, comparing the 5.25 μm band with the 3.4, 6.2, and 11.2 μm emission bands from NGC 7027 using the higher quality *ISO* SWS data. The major astronomical features at 6.2 and 11.2 μm arise from fundamental vibrations whereas the 5.25 μm band is produced by combinations and overtones involving fundamentals. The similarities between the profiles of these bands are striking, even down to the blue satellite features for the 6.2 and 11.2 μm bands. However, on an (absolute) energy scale the widths and skewness of the profiles show some variations, with the 6.2 μm profile clearly different. Both width and skewness are tied to the anharmonicity parameter of the transition involved, which depends on the involved mode (Joblin et al. 1995). While presently relevant spectroscopic data are lacking, we note that future experimental studies on the relevant modes may prove to be very insightful.

Roche et al. (1996) found that the ratio of the 11.2 μm band intensity to that of the 5.25 μm band was roughly constant

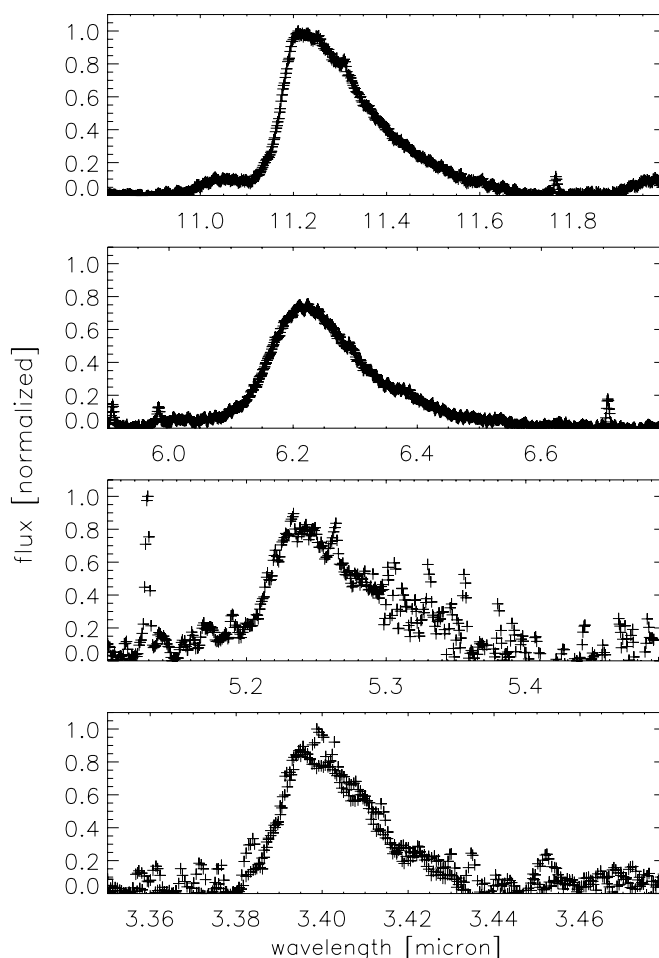


Figure 9. Comparison between the normalized profile of the 5.25 μm band to those of the normalized 3.4, 6.2, and 11.2 μm bands in NGC 7027; note the similarities.

(28–32) over their sample of three PNe. Here, from Table 3, the $I_{11.25}/I_{5.25}$ in HD 44179 and the two positions in Orion are about $10 (\pm 1.0)$, whereas it is $14 (\pm 1.5)$ in NGC 7027. We have developed a simple model to computationally determine this ratio based on the average (~ 9.5), experimentally established, (10–15)/5.25 μm cross sections of 15 neutral PAHs with 28–50 carbon atoms. The model predicts the $I_{11.25}/I_{5.25}$ ratio as a function of PAH size and photon excitation energies. The thermal approximation is used to determine the emission spectrum and radiative relaxation is taken into account (Dwek et al. 1997; Bakes et al. 2001). Figure 10 shows the predicted ratios as a function of PAH size between two different excitation energies, 8 and 10 eV. For average photon excitation energies of 8 and 10 eV, PAHs with about 40–65 carbon atoms produce the observed ratios for HD 44179 and the two positions in Orion. NGC 7027 implies that PAHs with between 65 to about 105 carbon atoms are required to match the observed ratio. This is very much in line with the estimate based on the 3.3/11.2 μm ratio (Allamandola et al. 1989b).

The analysis of the laboratory data and the quantum-chemical calculations point to the involvement of CH_{oop} modes for the emission between 5 and 6 μm . The good correlation between the 5.25/6.2 with the 11.2/6.2 μm band strength ratios ($R = 0.97$) and the 5.7/6.2 with the 11.2/6.2 μm band strength ratios ($R = 0.97$), which traces the CH modes, affirms this (Figure 11).

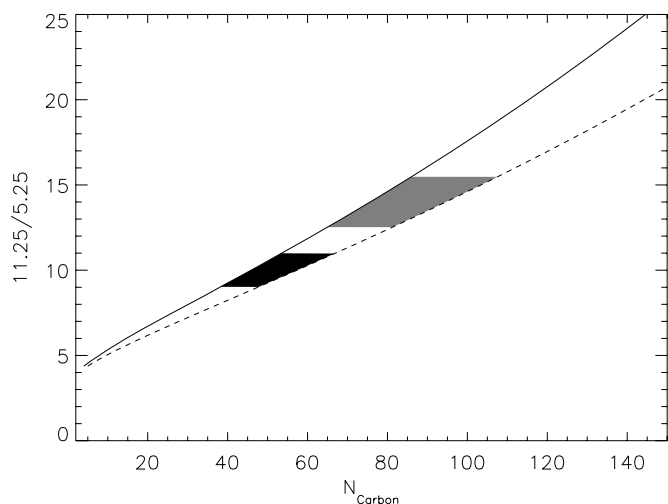


Figure 10. $I_{11.25}/I_{5.25}$ ratio as a function of neutral PAH size modeled using the thermal approximation and including radiative cooling. The solid line is the ratio for an average photo-excitation energy of 8 eV and the dashed line for an average photon energy of 10 eV. The black area is where the astronomically observed ratio of $\sim 10 (\pm 1.0)$ falls and the area in gray that where the observed ratio of $\sim 14 (\pm 1.5)$ falls.

In contrast, there is no good correlation between the 5.25/11.2 with the 6.2/11.2 μm ratios, showing again that the 5.25 μm and CC modes are not intimately connected in the astronomical spectra.

Ionization of PAH molecules can influence band positions, but not as notably as the effect on the relative band intensities. Upon ionization the strength of the CC modes increases significantly, while the CH modes tend to decrease in strength. However, there appears to be a size dependence to this. PAHs of a comparable size to those implied here do not have significant reduction in CH band strength (Bauschlicher et al. 2008). NGC 7027 and the two positions in the Orion Bar probe the two extremes in ionizing environments. Future studies on a larger sample will have to establish whether the difference in 5.25/11.2 μm ratio for NGC 7027 is a real property of the interstellar PAH spectra. While the theoretical data suggest that ionized PAHs and non- CH_{oop} modes may be involved, for now we conclude that the correlation in Figure 11 advocates for neutral carriers dominating the astronomical 5.25 μm PAH band.

Hony et al. (2001) made a study of the 10–15 μm region, the bands which are due to aromatic CH_{oop} vibrational modes. Laboratory data and quantum-chemical calculations show that the peak position of the bands in this region depends on the number of adjacent hydrogen atoms on the periphery of PAH molecules. Therefore, ratios of these bands will reveal the structure of the emitting PAHs in astronomical environments. The predominance of the 11.2 over 12.7 μm band intensity in the four sources investigated here points to compact carriers (Hony et al. 2001). Since the emission in the 5–6 μm region involves coupling with, and intensity borrowing from, the CH_{oop} modes, this also holds for the 5.25 and 5.7 μm bands. However, it is prudent to look at the 5–6 μm region of sources in which the 12.7 is as strong as the 11.2 μm band (e.g., IRAS 18317). Unfortunately good signal-to-noise spectra of the 5.25 μm band are not yet available for the sources known to show such ratios.

Lastly, the presence of quartets produces emission in-between and beyond the positions of the observed astronomical 5.25 and 5.7 μm features that excludes them as important parts of the astronomical PAH family (Hony et al. 2001). This is completely consistent with the conclusions about the PAH structures from the 10–15 μm region.

We turn now to the 5.7 μm band. Figure 6 illustrates the dependence of the 5.7 μm peak position on the molecular edge structure. As the laboratory data show, duos and trios cluster on the blue side whereas the presence of solos produce features on the red side of the feature. While the four spectra are quite similar, the spectrum of the Orion Bar position D5 seems to indicate that the duo and trio hydrogens are as important as solo hydrogens, even though both Orion Bar positions show similar 11.2/12.7 μm band strength ratios. The difference in the spectra between Orion Bar positions D5 and H2S1 suggests a different PAH population at both positions. This difference might be driven by erosion, where more irregular shaped PAHs are present at position D5.

All of the 15 initially considered astronomical spectra show emission features at 5.25 and 5.7 μm , but nothing significant in-between. This rules out a large population of quartet containing PAHs. The spectra span a significant range of astrophysical environments, suggesting that many, if not most, of the astronomical PAH population is dominated by large and compact PAHs. It bears repeating here that the greater intrinsic strength of the solo CH over that of duo CH is largely responsible for the

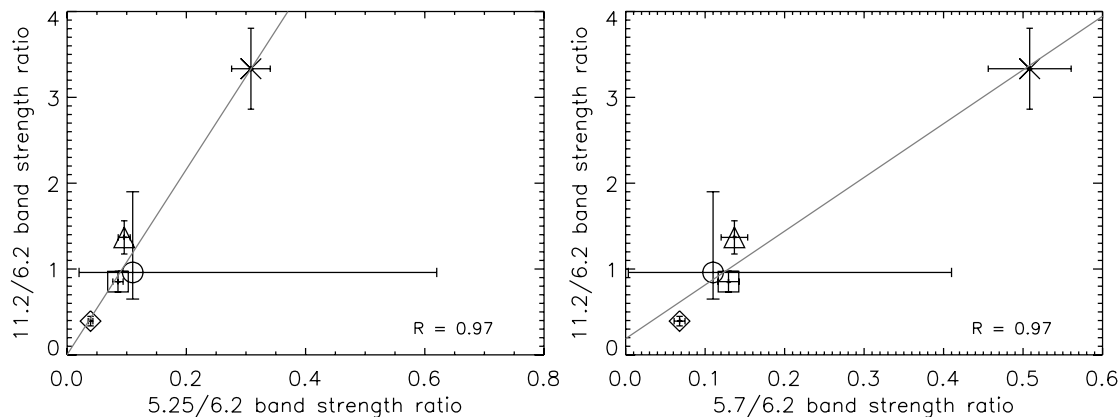


Figure 11. Band strength ratio correlations. (\diamond) HD 44179; (Δ) NGC 7027; (\square) Orion Bar H2S1; (\times) Orion Bar D5; (\circ) nearby galaxies (J. D. Smith 2007, private communication). Note that for the galaxies, the strength of the 5.25 μm band was determined by assuming a slightly asymmetric Drude profile with a width and wavelength center trained on a high S/N subset of the *Spitzer* Infrared Nearby Galaxies Survey (SINGS; Kennicutt et al. 2003) spectra. Integrating the full profile produces the used bands strength. Also note that some of the SINGS spectra have modest redshifts, which bring slightly more of the feature in view, up to roughly a quarter of the feature's FWHM.

predominance of the 11.2 μm astronomical band in the CH_{oop} region.

It has been shown by Peeters et al. (2002) that the variations in peak position and shape of the PAH bands in the 6–9 μm region can be grouped into distinctive classes. Moreover, these classes seem to correlate with object type. All ISM-like sources belong to class A. These are characterized by a CC-stretch band peaking at 6.2 μm and the “7.7” μm band complex peaking at 7.6 μm . On the other hand, isolated Herbig Ae/Be stars together with a few post-AGB stars and most PNe belong to class B. These are characterized by a CC-stretch band peaking between 6.24 and 6.28 μm and “7.7” μm band complex peaking between 7.8 and 8.0 μm . HD 44179, NG7027, and the two positions in the Orion Bar cover both of these classes, with HD 44179 and NGC 7027 representing class B and both positions in the Orion Bar representing class A. Interestingly enough, for the quality of the spectra available, the 5.25 and 5.7 μm features do not allow for such a classification, behavior consistent with CH modes. Given that the shift between class A and class B type of spectra seems strongly influenced by the relative populations of PAH cations to PAH anions (Bauschlicher et al. 2008), the apparent independence of the astronomical 5.25 and 5.7 μm bands from these classifications strongly suggests again that they track the neutral PAH population.

The spectrum labeled “galaxies” in Figure 3 presents the slightly redshifted average galaxy spectrum from Smith et al. (2007), obtained using *Spitzer*’s Infrared Spectrograph (IRS; Houck et al. 2004) and shows part—due to IRS’ cutoff at 5.2 μm —of the 5.25 μm band and the 5.7 μm band. Compared to *ISO*, *Spitzer* has limited spectral resolution but superior sensitivity. The spectrum demonstrates the accessibility of this region using *Spitzer* and therefore the possibility for band-strength analysis and, for the 5.7 μm band, studies of erosion processes as outlined in this paper.

5. SUMMARY AND CONCLUSION

This paper presents a study of the two minor PAH features in the 5–6 μm (2000–1667 cm^{-1}) region, centered at positions near 5.25 (1905 cm^{-1}) and 5.7 μm (1739 cm^{-1}). These contain information about the interstellar PAH population and conditions in the emission regions that both complement and extend the information revealed by the major bands.

Fifteen high-quality *ISO* SWS spectra have been investigated for emission in the this wavelength region, with four spectra having sufficient signal-to-noise to allow for an in-depth analysis. Combined with a spectral database comprised of laboratory studies and dedicated quantum-chemical calculations, these spectra allow us to probe the main characteristics of the carriers of the astronomical PAH features. After continuum and emission line removal, all four astronomical spectra show similar, almost universal profiles. However, the signal-to-noise level can be improved and there are hints of subtle, but interesting, variations.

The absence of bands between 5 and 6 μm in laboratory spectra of deuterated polycyclic aromatic molecules, as well as the absence of fundamentals in the quantum-chemical calculations in this region along with the strong correlation between the 5.25 and 5.75 μm band strength with the 11.2 μm band strength in the astronomical spectra, substantiates the involvement of CH_{ip} and CH_{oop} bending vibrations. In-depth analysis of the laboratory spectra and quantum-chemical calculations show that the astronomical 5.25 and 5.75 μm bands are a blend of combination, difference, and overtone bands, involving CH_{ip} and CH_{oop} bending and stretching modes and, likely for the larger ionized

PAHs, CC_{oop} modes. When it becomes possible to compute the intensities of overtone and combination bands, this work should be extended.

Turning to the hydrogen adjacency classes, PAHs with solo and duo hydrogens consistently produce prominent bands in the appropriate wavelength regions, whereas PAHs with higher adjacency hydrogens show far richer spectra. These produce bands in-between and beyond the 5.25 and 5.7 μm bands, ruling such species out as important members of the emitting population. The 5.7 μm feature in itself—through its profile—contains adjacency class information that might be more easily accessible than through the 10–15 μm CH_{oop} region, where it is difficult to separate the duo and trio hydrogen modes.

The data suggest that the emitting astronomical PAHs are mostly large ($50 \lesssim N_{\text{C}} \lesssim 100$), compact, and not fully deuterated. Furthermore, both the quantum-chemical calculations and the absence of a correlation between the 5.25/6.2 and 5.7/6.2 μm band strengths with the 11.2/6.2 μm band strength ratio suggest that the 5.25 and 5.7 μm PAH bands do not trace ionization and are carried predominately by neutrals. This point is reinforced by the lack of connection with class A and class B PAH band behavior. This suggests that high-quality spectra from 5 to 10 μm provide insight into the neutral as well as the cation and anion members of the emitting astronomical PAH family. Even so, a bigger collection of spectra of large compact PAHs, with mixtures of solo, duo, and trio hydrogens, is still needed to firm up these conclusions.

Christiaan Boersma acknowledges support from the Netherlands Organization for Scientific Research (NWO; grant R 78-405). The experimental aspects of this work were supported through NASA’s Long Term Space Astrophysics (grant 907524) and Astrobiology (grant 811073) Programs and earlier support from NASA’s Laboratory Astrophysics Program. Andrew Mattioda acknowledges the support of the National Research Council. As always, we are deeply indebted to Robert Walker for his outstanding technical support of all phases of the experimental work.

REFERENCES

- Allamandola, L. J., Bregman, J. D., Sandford, S. A., Tielens, A. G. G. M., Witteborn, F. C., Wooden, D. H., & Rank, D. 1989a, *ApJ*, **345**, L59
- Allamandola, L. J., & Hudgins, D. M. 2003, in *Solid State Astrochemistry*, ed. V. Pirronello, J. Krelowski, & G. Manicò (Dordrecht: Kluwer), 251–316
- Allamandola, L. J., Tielens, A. G. G. M., & Barker, J. R. 1989b, *ApJS*, **71**, 733
- Bakes, E. L. O., Tielens, A. G. G. M., & Bauschlicher, C. W. 2001, *ApJ*, **556**, 501
- Barone, V. 2005, *J. Chem. Phys.*, **122**, 014108
- Bauschlicher, Jr., C. W. 2002, *ApJ*, **564**, 782
- Bauschlicher, Jr., C. W., & Langhoff, S. R. 1997, *Spectrochim. Acta A*, **53**, 1225
- Bauschlicher, Jr., C. W., Peeters, E., & Allamandola, L. J. 2008, *ApJ*, **678**, 316
- Becke, A. D. 1993, *J. Chem. Phys.*, **98**, 5648
- Beintema, D. A., et al. 1996, *A&A*, **315**, L369
- Bellamy, L. J. 1960, *The Infrared Spectra of Complex Molecules* (New York: Wiley)
- Cane, E., Miani, A., & Trombetti, A. 2007, *J. Phys. Chem. A*, **111**, 8218
- de Graauw, T., et al. 1996, *A&A*, **315**, L49
- Draine, B. T., & Li, A. 2007, *ApJ*, **657**, 810
- Dwek, E., et al. 1997, *ApJ*, **475**, 565
- Frisch, M. J., Pople, J. A., & Binkley, J. S. 1984, *J. Chem. Phys.*, **80**, 3265
- Frisch, M. J., et al. 2004, Gaussian 03, Revision C.02 (Wallingford, CT: Gaussian, Inc.)
- Herzberg, G. 1945, *Molecular Spectra and Molecular Structure* (New York: Van Nostrand)
- Hony, S., Van Kerckhoven, C., Peeters, E., Tielens, A. G. G. M., Hudgins, D. M., & Allamandola, L. J. 2001, *A&A*, **370**, 1030

- Houck, J. R., et al. 2004, *ApJS*, **154**, 18
- Hudgins, D. L., & Allamandola, L. J. 1995a, *J. Phys. Chem.*, **99**, 3033
- Hudgins, D. L., & Allamandola, L. J. 1995b, *J. Phys. Chem.*, **99**, 8978
- Hudgins, D. M., & Allamandola, L. J. 1999, *ApJ*, **516**, L41
- Hudgins, D. M., & Allamandola, L. J. 2004, in ASP Conf. Ser. 309, *Astrophysics of Dust*, ed. A. N. Witt, G. C. Clayton, & B. T. Draine (San Francisco, CA: ASP), **665**
- Hudgins, D. M., Bauschlicher, Jr., C. W., & Allamandola, L. J. 2005, *ApJ*, **632**, 316
- Hudgins, D. L., & Sandford, S. A. 1998, *J. Phys. Chem. A*, **102**, 329
- Hudgins, D. L., Sandford, S. A., & Allamandola, L. J. 1994, *J. Phys. Chem.*, **98**, 4243
- Joblin, C., Boissel, P., Leger, A., D'Hendecourt, L., & Defourneau, D. 1995, *A&A*, **299**, 835
- Kennicutt, Jr., R. C., et al. 2003, *PASP*, **115**, 928
- Latter, W. B., Dayal, A., Biegging, J. H., Meakin, C., Hora, J. L., Kelly, D. M., & Tielens, A. G. G. M. 2000, *ApJ*, **539**, 783
- Li, A., & Draine, B. T. 2001, *ApJ*, **554**, 778
- Mattioda, A. L., Hudgins, D. M., Bauschlicher, Jr., C. W., & Allamandola, L. J. 2005, *Adv. Space. Res.*, **36**, 156
- Mattioda, A. L., Hudgins, D. M., Bauschlicher, Jr., C. W., Rosi, M., & Allamandola, L. J. 2003, *J. Phys. Chem. A*, **107**, 1486
- Oomens, J., van Roij, A. J. A., Meijer, G., & von Helden, G. 2000, *ApJ*, **542**, 404
- Pech, C., Joblin, C., & Boissel, P. 2002, *A&A*, **388**, 639
- Peeters, E., Hony, S., Van Kerckhoven, C., Tielens, A. G. G. M., Allamandola, L. J., Hudgins, D. M., & Bauschlicher, C. W. 2002, *A&A*, **390**, 1089
- Peeters, E., Mattioda, A. L., Hudgins, D. M., & Allamandola, L. J. 2004, *ApJ*, **617**, L65
- Portmann, S., & Lüthi, H. P. 2000, *CIMIA*, **54**, 766
- Rapacioli, M., Calvo, F., Joblin, C., Parneix, P., Toublanc, D., & Spiegelman, F. 2006, *A&A*, **460**, 519
- Roche, P. F., Lucas, P. W., & Geballe, T. R. 1996, *MNRAS*, **281**, L25
- Sellgren, K., Uchida, K. I., & Werner, M. W. 2007, *ApJ*, **659**, 1338
- Smith, J. D. T., et al. 2007, *ApJ*, **656**, 770
- Stephens, P. J., Devlin, F. J., Chabalowski, C. F., & Frisch, M. J. 1994, *J. Phys. Chem.*, **98**, 11623
- Tielens, A. G. G. M. 2008, *ARA&A*, **45**, 289
- van Dienenhoven, B., Peeters, E., Van Kerckhoven, C., Hony, S., Hudgins, D. M., Allamandola, L. J., & Tielens, A. G. G. M. 2004, *ApJ*, **611**, 928
- van Dishoeck, E. F. 2004, *ARA&A*, **42**, 119
- Van Kerckhoven, C., et al. 2000, *A&A*, **357**, 1013
- Verstraete, L., et al. 2001, *A&A*, **372**, 981
- Waelkens, C., et al. 1996, *A&A*, **315**, L245
- Yan, L., et al. 2005, *ApJ*, **628**, 604
- Young, C. W., DuVall, R. B., & Wright, N. 1951, *Anal. Chem.*, **23**, 709